

Electric-field-induced magnetic toroidal moment in a time-reversal-odd antiferromagnet

Takeshi Hayashida,¹ Koei Matsumoto,¹ Tsuyoshi Kimura¹

¹Department of Applied Physics, University of Tokyo, Bunkyo-ku, Tokyo 113-8656, Japan

Abstract

Recently, antiferromagnets with broken time-reversal (T) symmetry have been found to exhibit ferromagnet-like behaviors (e.g., anomalous Hall effect) despite the absence of net magnetization. However, antiferromagnets characterized by T -odd “scalar” quantities are expected to exhibit unique properties different from the ferromagnet-like behavior. One such example is the diagonal electrotoroidic (ET) effect, in which the application of an electric field E induces a magnetic toroidal moment, an ordered arrangement of magnetic vortices, in the direction parallel to E . Herein, we report the observation of the diagonal ET effect probed by E -induced nonreciprocal directional dichroism in Co_2SiO_4 holding a T -odd scalar quantity, magnetic toroidal monopole. Using the ET effect, a pair of domain states related to one another by the T operation is spatially resolved. Furthermore, we reveal the inversion of the domain pattern by a magnetic field, which is explained by trilinear coupling ascribed to the piezomagnetic effect. Our observation of the diagonal ET effect paves the way for the exploration of unique functionalities of T -odd antiferromagnets.

Main

Antiferromagnetism is a state in which magnetic moments are ordered in a way that the overall magnetization is canceled out. Although Louis Néel¹, who was awarded the Nobel Prize for research on antiferromagnetism in 1970, described it as “interesting but useless,” a considerable amount of research since his comment has revealed that certain antiferromagnets exhibit unique functionalities or physical phenomena. These properties often arise from the breaking of time-reversal (T) symmetry. For example, in an insulating antiferromagnet where space-inversion (P) and T symmetries are simultaneously broken but the combined PT symmetry is preserved, the linear magnetoelectric (ME) effect emerges²⁻⁴. Such ME antiferromagnets also exhibit unique nonreciprocal optical and transport properties⁵. For another example, recent investigations have revealed that antiferromagnets breaking T and PT symmetries show physical properties that are usually observed in ferromagnets, including the anomalous Hall effect, magneto-optical Kerr effect, and nonrelativistic spin splitting, despite the absence of (or tiny) net magnetization⁶⁻¹³. To understand such unconventional properties in T - and PT -odd antiferromagnets with collinear and compensated magnetism, a novel concept termed “altermagnetism” has been introduced; notably, altermagnetism has already attracted extensive interest^{14,15}. Herein, we examine another unique physical property of T - and PT -odd antiferromagnets, especially those characterized by T - and PT -odd “scalar” quantity, i.e., the diagonal electrotoroidic (ET) effect, where the application of \mathbf{E} induces magnetic toroidal moment in the direction parallel to \mathbf{E} . The diagonal ET effect was proposed in the 2000s^{16,17}, but has not been experimentally investigated to date.

The magnetic toroidal moment \mathbf{T} is a T -odd polar vector that describes vortex arrangements of magnetic

dipoles as $\mathbf{T} \propto \sum_i \mathbf{r}_i \times \mathbf{m}_i$, where \mathbf{r}_i is the position vector of the magnetic dipole \mathbf{m}_i at the i site with reference to the high symmetry point (the middle panel of Fig.1). The spontaneous order of magnetic toroidal moments, so-called ferrotoroidic order, has long been discussed theoretically^{16,18-20}, and ferrotoroidic domains were experimentally observed using optical second harmonic generation in 2007²¹. In parallel with the discussion on the ferrotoroidic order, Schmid introduced a linear response of \mathbf{T} to applied \mathbf{E} , described as $T_i = \theta_{ij}E_j$ and termed it the ET effect^{16,17}. Here, θ_{ij} is a second rank T -odd polar tensor called the ET tensor. Note that the ET effect is a phenomenon ascribed to a bi-linear ME coupling since \mathbf{T} is symmetrically equivalent to $\mathbf{H} \times \mathbf{E}$ and the coupling between \mathbf{T} and \mathbf{E} is expressed as $(\mathbf{H} \times \mathbf{E})_i E_j$ ¹⁶. When $i \neq j$ and $i = j$, the effect is off-diagonal ($\mathbf{E} \perp \mathbf{T}$) and diagonal ($\mathbf{E} \parallel \mathbf{T}$), respectively. Off-diagonal coupling is rather common and is observed in systems breaking both P and T symmetries with the cross product of spontaneous (or field-induced) \mathbf{M} and an applied \mathbf{E} , i.e., $\mathbf{T} \propto \mathbf{M} \times \mathbf{E}$ (the right panel of Fig. 1). The off-diagonal ET effect has been observed through nonreciprocal optical phenomena in systems with \mathbf{E} and a magnetic field \mathbf{H} applied in perpendicular directions ($\mathbf{T} \propto \mathbf{H} \times \mathbf{E}$)²². On the other hand, for the emergence of the diagonal ET effect, \mathbf{T} is induced as a result of changing only the T symmetry while maintaining the direction of \mathbf{E} , which should be observed in systems holding a T -odd “scalar” quantity. Recently, Hayami and Kusunose showed that such a class is characterized by “magnetic toroidal monopole”, that is, all-in or all-out arrangements of the local magnetic toroidal moment²³ (the left panel of Fig. 1). Considering symmetry, 32 magnetic point groups allow for the emergence of the magnetic toroidal monopole and therefore the diagonal ET effect²³. More recently, a similar classification focusing on spontaneous and field-induced \mathbf{T} has been introduced by Xu and coworkers²⁴. We note that there is an overlap between the systems described by the magnetic octupole and the magnetic toroidal monopole^{25,26}. However, the magnetic octupole includes both the systems that allow for ferromagnet-like behaviors (e.g., Mn_3Sn ²⁷) and those characterized by T -odd scalar quantity, like Co_2SiO_4 . In this research, we focus on the latter, and thus we adopt the classification using the magnetic toroidal monopole.

Time-reversal-symmetry-broken antiferromagnet Co_2SiO_4

To observe the diagonal ET effect, we selected Co_2SiO_4 as the target material. Co_2SiO_4 crystalizes in the olivine structure (space group $Pnma$, Fig. 2a)²⁸⁻³⁰. Co^{2+} ions are surrounded by six O^{2-} ions and occupy two different octahedral sites: Co1 located at the centrosymmetric site (site symmetry $\bar{1}$) and Co2 located at the mirror-symmetric site whose mirror plane is perpendicular to the b axis (site symmetry m). Co_2SiO_4 shows an antiferromagnetic (AFM) transition at $T_N = 50 \text{ K}$ ³¹⁻³³. In the AFM phase, spins on the Co2 sites are collinearly aligned along the b axis, whereas those on the Co1 sites are slightly tilted from the b axis and form zigzag spin chains (red arrows in Fig. 2a). The magnetic point group is mmm , which permits the diagonal ET effect with the nonzero distinct ET tensor components of θ_{11} , θ_{22} , and θ_{33} ³⁴. Although the noncollinear spins on the Co1 sites are also related to the breaking of T symmetry²⁴, herein, we focused on the collinear spins on the Co2 site for simplification. As mentioned above, \mathbf{T} describes vortex arrangements of multiple magnetic dipoles; however, local magnetic toroidal moment \mathbf{t} can also be defined at a single ion site by considering the cross product of a local electric dipole moment \mathbf{p} and a local magnetic moment \mathbf{m} , as $\mathbf{t} \propto \mathbf{p} \times \mathbf{m}$ ³⁵. At the Co2 site with \mathbf{m}_{Co2} (red arrows in Fig. 2b), an inversion symmetry is locally broken while a mirror symmetry perpendicular to the b axis

is preserved, and thus \mathbf{p}_{Co_2} emerges in the ac plane (orange arrows in Fig. 2b). Then, a local magnetic toroidal moment at the Co2 site, \mathbf{t}_{Co_2} ($\propto \mathbf{p}_{\text{Co}_2} \times \mathbf{m}_{\text{Co}_2}$) is introduced (magenta arrows in Fig. 2b). Note that the sum of \mathbf{t}_{Co_2} is canceled out in a unit cell with four Co2 sites; therefore, Co_2SiO_4 is not ferrotoroidic ($\mathbf{T} = \mathbf{0}$) in the absence of \mathbf{E} . In contrast, when applying \mathbf{E} , for example, along the a (or c) axis, the sum of \mathbf{p}_{Co_2} and accordingly that of \mathbf{t}_{Co_2} are no longer canceled out, making \mathbf{T} finite in the direction parallel to \mathbf{E} . Thus, Co_2SiO_4 shows the diagonal ET effect.

In the absence of \mathbf{E} , the structure of Co_2SiO_4 does not show finite \mathbf{T} but holds a T -odd scalar quantity, that is, magnetic toroidal monopole ($\propto \sum_i \mathbf{r}_i \cdot \mathbf{t}_i$)²³. One can consider the two domain states related to each other by the T operation, termed E_{T+} and E_{T-} domains (left and right panels of Fig. 2b), which are characterized by the magnetic toroidal monopole with positive ($\sum_i \mathbf{r}_i \cdot \mathbf{t}_i > 0$) and negative ($\sum_i \mathbf{r}_i \cdot \mathbf{t}_i < 0$) divergence, respectively. We also note that spin-up and spin-down sublattices are related to each other by glide operations but not by space-inversion or translation, which is nothing more or less than the definition of altermagnetism^{14,15}, i.e., Co_2SiO_4 is an altermagnet from the perspective of the symmetry^{36,37}.

Electric-field-induced nonreciprocal directional dichroism

The sign of the ET tensors of the two E_T domain states are opposite, indicating that these states exhibit \mathbf{T} with opposite polarities ($T+$ and $T-$) under \mathbf{E} . The way to align the system into a single domain state is nontrivial and has not yet been established, which severely complicates the observation of the ET effect through the measurement of macroscopic physical quantities. Thus, the optimal approach for observing the ET effect is the visualization of domain structures through spatial distribution measurements. To this end, we adopted nonreciprocal directional dichroism (NDD), i.e., asymmetry in optical absorption between two counterpropagating light beams. NDD has been observed in ferrotoroidic materials and materials in which magnetic toroidal moment is induced by the cross product of \mathbf{E} (\mathbf{P}) and \mathbf{H} (\mathbf{M})^{35,38–40}. Because the states with $T+$ and $T-$ show different absorption, NDD has been used to visualize ferrotoroidic domains^{41,42}. Taking NDD and the diagonal ET effect into account, the absorption coefficient α [cm^{-1}] of the AFM phase of Co_2SiO_4 under \mathbf{E} can be described as

$$\alpha = \alpha_0 + \Delta\alpha = \alpha_0 + \beta(\mathbf{k} \cdot \mathbf{E}), \quad (1)$$

where α_0 is an absorption coefficient without \mathbf{E} , $\Delta\alpha$ is the difference in the absorption coefficient induced by \mathbf{E} , β is the coefficient describing the electric-field-induced (E -induced) NDD whose sign depends on the E_T domain state, and \mathbf{k} is the light propagation vector. When \mathbf{E} is parallel to \mathbf{k} , the intensity of the transmitted light I is described as

$$I = I_0 e^{-(\alpha_0 + \Delta\alpha)d} \approx I_0 e^{-\alpha_0 d} (1 - \Delta\alpha d) = I_0 e^{-\alpha_0 d} (1 - \beta V), \quad (2)$$

where I_0 is the intensity of the incident light, d [cm] is the sample thickness, and $V = Ed$ [V] is the applied voltage. In the transformation of Eq. 2, $\Delta\alpha d$ is assumed to be small. Under this approximation, the change in transmitted light intensity due to the ET effect is linear relative to V . By obtaining spatial maps of this E -induced NDD, E_T domains will be visualized, which manifests the diagonal ET effect (Fig. 2c). Note that E -induced NDD has also been suggested as a tool for observing the diagonal ET effect in ref. ²⁴.

Observation of diagonal ET effect via E -induced NDD

We measured E -induced NDD of Co_2SiO_4 single crystals. For the measurements in the transmittance

geometry, we prepared three thin samples whose widest faces are parallel to the (100), (010), and (001) planes (Methods). Based on other E -induced optical effects in magnetic materials (e.g., E -induced magnetic circular dichroism in Cr_2O_3 ⁴³), E -induced NDD signals are expected to be weak. Thus, we adopted an electric-field-modulation imaging technique⁴⁴, which enables us to detect the spatial distribution of E -induced NDD signals with high sensitivity (Methods). Figures 3a-c, e-g, and i-k show the maps of $\Delta\alpha d$ obtained in the geometry where both \mathbf{k} and \mathbf{E} are along the a , b , and c axes, respectively, at selected V . The images were obtained at 4 K ($< T_N$) using unpolarized light with wavelengths of 550 nm (Figs. 3a-c and i-k) and 590 nm (Figs. 3e-g). In all the samples, a clear contrast of red and blue corresponding to the positive and negative $\Delta\alpha$, respectively, is observed at 200 V (Figs. 3c, g, k). The color contrasts monotonically increase with voltage. We calculated the average $\Delta\alpha d$ for the pixels at selected single domain areas (both positive and negative $\Delta\alpha d$) denoted by boxes in Figs. S1a-c and determined the V dependence of $\Delta\alpha d$. As shown in Figs. 3d, h, l, $\Delta\alpha d$ is linear with respect to V . We also checked that the contrasts disappeared at temperatures above T_N (Extended Data Fig. 1). Furthermore, the lock-in measurements with a focused laser beam in a detailed temperature range (Methods) confirm that the E -induced NDD disappears above T_N (Extended Data Fig. 2). Consequently, the obtained contrasts are pairs of E_T domains showing the opposite sign of E -induced NDD, and, namely, we succeeded in observing the diagonal ET effect. The effect is observed in all the settings of $\mathbf{E}||\mathbf{k}||a, b, c$, suggesting that all the diagonal ET tensor components (θ_{11} , θ_{22} , and θ_{33}) are finite, which is consistent with the magnetic point group mmm . Note that the signs of the domain states between the different planes cannot be uniquely associated in the present measurements; thus, the color (the sign of $\Delta\alpha$) coincidence of the domains between Figs. 3c, g, and k does not necessarily indicate the coincidence of the domain states.

The domain sizes on the (100) and (001) planes (Figs. 3c, k) are on the order of several hundred micrometers, whereas that on the (010) plane (Fig. 3g) is on the order of several tens of micrometers. The domains on the (010) plane are expected to be vertically cut from the domains on the (100) and (001) faces along the b axis, which does not match the experimental results. As discussed below, the domains of Co_2SiO_4 are probably related to strain, and the domain size may be affected by residual strains induced during sample preparation, particularly, cutting and polishing.

We have also acquired the spectra of E -induced NDD by focusing a laser beam on a single domain region and using a lock-in technique (Methods). Although NDD itself does not depend on the polarization of incident light, polarization affects the absorption and E -induced NDD because of the orthorhombic crystal structure. Therefore, the measurements were performed using linearly polarized light. Complex peak structures of E -induced NDD were observed in the energy range the Co d - d transition (Extended Data Fig. 3)⁴⁵. For a detailed analysis and discussion of the spectra, see Supplementary Note 1 and Figure S2.

Domain inversion by applying a magnetic field

Because the magnetic point group mmm of Co_2SiO_4 forbids spontaneous magnetization, the E_T domains were expected to not respond to a magnetic field \mathbf{H} . However, the domains exhibited an anomalous response to \mathbf{H} . Figure 4 shows the domain maps on the (100) plane obtained at 4 K in the absence of \mathbf{H} after cooling the samples across T_N while applying \mathbf{H} of ± 50 mT along the c (Figs. 4a, b), b (Figs. 4c, d) and a (Figs. 4e, f) axes. The domain strongly depends on the direction of the cooling \mathbf{H} . However, a single domain has never been obtained

in any \mathbf{H} direction. The most surprising feature is that the domain contrasts are completely inverted by reversing the direction of cooling \mathbf{H} while maintaining the positions of the domain boundaries [compare Fig. 4a with 4b (or Fig. 4c with 4d, Fig. 4e with 4f)]. We also checked how the domains respond when \mathbf{H} is applied below T_N (Supplementary Note 3). Figure S3 shows the result for the (100) plane sample at 49 K (just below T_N) in $\mathbf{H}\parallel c$. The application of \mathbf{H} changes the domain structure, and, again, the domain contrast was inverted depending on the sign of \mathbf{H} .

This domain inversion in response to the flipping of the sign of \mathbf{H} provides insights into the mechanism of the unexpected response of the E_T domains. Similar domain inversion has been reported in some multiferroics (e.g., Mn_2GeO_4 and $Dy_{0.7}Tb_{0.3}FeO_3$) in which three order parameters (AFM order parameter L , magnetization M , and electric polarization P) are coupled via a trilinear coupling, and the Landau free energy is described as $F \propto -LMP$ ⁴⁶⁻⁴⁸. When one of the order parameters, e.g., L , is fixed, the other two (M and P) are coupled to minimize the free energy, and the domain switching of M accompanies that of P . In this case, the domain pattern of P is clamped by that of L , but the sign of P in each domain is inverted in response to a sign reversal of M .

In the case of the T -odd antiferromagnet Co_2SiO_4 , L is the only well-defined order parameter, which is equivalent to the order parameter of the E_T domain. However, considering the observed response to \mathbf{H} , magnetization can be another order parameter. In fact, our magnetization measurements revealed tiny spontaneous magnetization below T_N (Extended Data Fig. 4). Although the observed spontaneous magnetization is very small (on the order of 10^{-4} μ_B /f.u.), its emergence contradicts the magnetic point group of Co_2SiO_4 .

Here we consider that the origin of magnetization is ascribed to “a linear piezomagnetic effect”, a linear coupling between magnetization and strain σ , which is permitted in T -odd antiferromagnets characterized by the magnetic toroidal monopole or magnetic octupole⁴⁹. In fact, the piezomagnetic effect is observed in several T -odd antiferromagnets, including the spin reorientation phase of $DyFeO_3$ ⁵⁰ whose magnetic point group is mmm and the same as Co_2SiO_4 . The linear piezomagnetic effect is defined as $M_i = \Lambda_{ijk}\sigma_{jk}$ ⁵¹⁻⁵³ where Λ_{ijk} is a piezomagnetic tensor. In the magnetic point group mmm , Λ_{abc} , Λ_{bca} , and Λ_{cab} are finite, and their sign depends on the E_T domain state³⁴. Thus, if there is an internal shear strain in Co_2SiO_4 , a trilinear coupling described as $F = -M_i\sigma_{jk}L$ is expected. This strain may be induced by cutting or polishing the sample and/or intrinsic distortion of the crystal lattice. When shear-strain domains are spatially distributed and remain unchanged during the application of \mathbf{H} , the observed inversion of E_T domains caused by the application of \mathbf{H} is well explained (Fig. 5). Because the application of \mathbf{H} transforms the M domain into a single domain state, the shear-strain and E_T domains are clamped, and a reversal of M leads to the inversion of E_T . The direction of \mathbf{H} determines which shear-strain distributions respond (σ_{ab} for H_c , σ_{ca} for H_b , and σ_{bc} for H_a). Thus, as observed in our sample, the E_T domain structure depends on the direction of \mathbf{H} (compare Figs. 4a, 4c and 4e). The presence of the strain domains in our samples was not confirmed experimentally. In an antiferromagnet CoF_2 , the piezomagnetic effect due to shear stress is observed⁵². If the piezomagnetic coefficient of Co_2SiO_4 is comparable to that of CoF_2 , the internal strain in our samples is estimated to be several MPa based on the observed spontaneous magnetization.

Conclusion

In conclusion, we investigated the diagonal ET effect in the T -odd antiferromagnet Co_2SiO_4 . This effect is

unique to materials characterized by the order of the T -odd scalar quantity, such as the magnetic toroidal monopole. In such materials, the anomalous Hall effect and the magneto-optical Kerr effect do not manifest, for which reason these materials have been less investigated. As proved in this study, the diagonal ET effect and the resulting E -induced NDD are highly effective means of revealing the hidden order. The diagonal ET effect occurs in an insulator to which an electric field can be applied. Until now, discussions on T - and PT -odd antiferromagnets, particularly those centered on altermagnets, have mainly focused on metallic systems^{14,15}. Our research contributes to the extension of such studies to insulators. Candidate materials are DyFeO_3 ⁵⁰ and Mn_2GeO_4 ⁴⁶.

We also revealed a unique domain inversion in Co_2SiO_4 under a magnetic field, which can be explained by a trilinear coupling mediated by the piezomagnetic effect. This suggests that E_T domains can be controlled through the simultaneous application of shear stress and a magnetic field. Furthermore, in systems where the piezomagnetic effect is permitted, magnetic linear dichroism emerges⁵³, and as its inverse effect, E_T domains may be controlled via irradiation with linearly polarized light in a magnetic field⁵⁴.

Finally, we comment on the term “electrotoroidic effect” which represents a linear response of a magnetic toroidal moment to an applied electric field. The term was introduced by Schmid in the 2000s^{15,16}. At that time, the term “toroidal moments” represents only magnetic toroidal moments. Recently, however, there have been renewed discussions of “electric toroidal moments” from the perspective of order parameters for ferroaxial order and chirality^{26,55}. In this context, the term “electro-magnetotoroidic effect” may represent the phenomenon studied here precisely.

Methods

Sample preparation

A Co_2SiO_4 single crystal was grown by the floating zone method⁵⁶. The obtained crystal was oriented using Laue x-ray diffraction, and three plate-shaped samples with the widest faces perpendicular to the a , b , and c axes were prepared. For the transmittance optical measurements under an electric field, the plate-shaped samples were polished to a thickness of 50–90 μm , and indium–tin oxide was sputtered onto the widest faces of the samples to form a pair of transparent electrodes. Magnetization was measured using a commercial physical property measurement system (PPMS, Quantum Design).

Spatial distribution measurements of E -induced NDD

Two-dimensional maps of the E -induced NDD were obtained by using an electric-field-modulation imaging technique⁴⁴. In these measurements, a square-wave voltage was applied to a sample, and transmission microscope images were captured using an sCMOS camera (pco edge 5.5, PCO) under alternating positive ($+V$) and negative ($-V$) voltages. Then, the difference in signals under $+V$ and $-V$ [$\Delta I = I(+V) - I(-V)$] divided by their average (I) was calculated for each pixel. Using equations (1) and (2), $\Delta I/I$ may be expressed as

$$\frac{\Delta I}{I} \cong \frac{I_0 e^{-\alpha_0 d} (1 - \Delta \alpha d) - I_0 e^{-\alpha_0 d} (1 + \Delta \alpha d)}{\{I_0 e^{-\alpha_0 d} (1 + \Delta \alpha d) + I_0 e^{-\alpha_0 d} (1 - \Delta \alpha d)\}/2} = -2\Delta \alpha d = -2\beta V \quad (3)$$

To obtain spatial distributions of small signals of $\Delta I/I$ while minimizing noise, large numbers (5,000 ~ 15,000)

of $\Delta I/I$ maps were captured and averaged. A square-wave bias voltage was applied at a frequency of 20 Hz, and images were captured at 40 fps.

The sample temperature was controlled using a liquid He flow cryostat (Microstat He, Oxford Instruments). Domain imaging under a magnetic field was performed using an electromagnet (3470, GMW associate).

Spectral measurements of optical absorption and E -induced NDD

Optical absorption spectra and E -induced NDD spectra were measured using a supercontinuum laser (SC-Pro, YSL Photonics) and an acousto-optic wavelength tunable filter (AOTF-PRO, YSL Photonics). The spectra were measured by varying the wavelength of the incident linearly polarized light in 1 nm increments. In the absorption spectrum measurements, the intensity of light transmitted through the sample was measured and normalized using the intensity of light transmitted through only the window. In the E -induced NDD spectrum measurements, signals were detected using a lock-in technique. A sinusoidal voltage $V_0 \sin(2\pi ft)$ was applied, where $V_0 = 150$ V and $f = 999$ Hz. Under such a sinusoidal voltage, the intensity of the transmitted light may be expressed as

$$I_0 e^{-(\alpha_0 + \beta V_0 \sin(2\pi ft)/d)d} \approx I_0 e^{-\alpha_0 d} (1 - \beta V_0 \sin(2\pi ft)) \quad (4).$$

Then, the intensity of transmitted light oscillating at the frequency f was detected by using a lock-in amplifier, and $\Delta\alpha \equiv \beta V_0/d$ was calculated. The E -induced NDD spectra were measured at both E_{T+} and E_{T-} domains by focusing the laser to a point smaller than the domain size (beam size ~ 50 μm). In the same manner with the spatial distribution measurements, the sample temperature was controlled using the liquid He flow cryostat.

References

1. Néel, L. Magnetism and local molecular field. *Science* **174**, 985–992 (1971).
2. Dzyaloshinskii, I. E. On the magneto-electrical effect in antiferromagnetics. *Zh. Exp. Teor. Fiz.* **33**, 881–882 (1959).
3. Folen, V. J., Rado, G. T. & Dtalder, E. W. Anisotropy of the mangetoelectric effect in Cr_2O_3 . *Phys. Rev. Lett.* **6**, 607–608 (1961).
4. Spaldin, A. N. & Fiebig, M. The Renaissance of Magnetoelectric Multiferroics. *Science* **309**, 391–392 (2005).
5. Tokura, Y. & Nagaosa, N. Nonreciprocal responses from non-centrosymmetric quantum materials. *Nat. Commun.* **9**, 3740 (2018).
6. Nakatsuji, S., Kiyohara, N. & Higo, T. Large anomalous Hall effect in a non-collinear antiferromagnet at room temperature. *Nature* **527**, 212–215 (2015).
7. Šmejkal, L., MacDonald, A. H., Sinova, J., Nakatsuji, S. & Jungwirth, T. Anomalous Hall antiferromagnets. *Nature Reviews Materials* **7**, 482–496 (2022).
8. Šmejkal, L., González-Hernández, R., Jungwirth, T. & Sinova, J. Crystal time-reversal symmetry breaking and spontaneous Hall effect in collinear antiferromagnets. *Sci. Adv.* **6**, eaaz8809 (2020).
9. Feng, Z. *et al.* An anomalous Hall effect in altermagnetic ruthenium dioxide. *Nature Electronics* **5**, 735–743 (2022).
10. Feng, W., Guo, G. Y., Zhou, J., Yao, Y. & Niu, Q. Large magneto-optical Kerr effect in noncollinear antiferromagnets Mn_3X ($\text{X}=\text{Rh}, \text{Ir}, \text{Pt}$). *Phys. Rev. B* **92**, 144426 (2015).
11. Higo, T. *et al.* Large magneto-optical Kerr effect and imaging of magnetic octupole domains in an antiferromagnetic metal. *Nat. Photonics* **12**, 73–78 (2018).
12. Krempaský, J. *et al.* Altermagnetic lifting of Kramers spin degeneracy. *Nature* **626**, 517–522 (2024).
13. Naka, M. *et al.* Spin current generation in organic antiferromagnets. *Nat. Commun.* **10**, 4305 (2019).
14. Šmejkal, L., Sinova, J. & Jungwirth, T. Beyond Conventional Ferromagnetism and Antiferromagnetism: A Phase with Nonrelativistic Spin and Crystal Rotation Symmetry. *Phys. Rev. X* **12**, 031042 (2022).
15. Šmejkal, L., Sinova, J. & Jungwirth, T. Emerging Research Landscape of Altermagnetism. *Phys. Rev. X* **12**, 040501 (2022).
16. Schmid, H. On ferrotoroidics and electrotoroidic, magnetotoroidic and piezotoroidic effects. *Ferroelectrics* **252**, 41–50 (2001).
17. Schmid, H. Some symmetry aspects of ferroics and single phase multiferroics. *J. Phys. Condens. Matter* **20**, 434201 (2008).
18. Ginzburg, V. L., Gorbatsevich, A. A., Kopayev, Y. V. & Volkov, B. A. On the problem of superdiamagnetism. *Solid State Commun.* **50**, 339–343 (1984).
19. Dubovik, V. M. & Tugushev, V. V. Toroid moments in electrodynamics and solid-state physics. *Phys. Rep.* **187**, 145–202 (1990).
20. Gorbatsevich, A. A. & Kopayev, Y. V. Toroidal order in crystals. *Ferroelectrics* **161**, 321–334 (1994).
21. Van Aken, B. B., Rivera, J. P., Schmid, H. & Fiebig, M. Observation of ferrotoroidic domains. *Nature* **449**,

702–705 (2007).

22. Rikken, G. L. J. A., Strohm, C. & Wyder, P. Observation of magnetoelectric directional anisotropy. *Phys. Rev. Lett.* **89**, 133005 (2002).
23. Hayami, S. & Kusunose, H. Time-reversal switching responses in antiferromagnets. *Phys. Rev. B* **108**, L140409 (2023).
24. Xu, X., Huang, F.-T. & Cheong, S.-W. Magnetic toroidicity. *J. Phys. Condens. Matter* **36**, 203002 (2024).
25. Yatsushiro, M., Kusunose, H. & Hayami, S. Multipole classification in 122 magnetic point groups for unified understanding of multiferroic responses and transport phenomena. *Phys. Rev. B* **104**, 054412 (2021).
26. Winkler, R. & Zülicke, U. Theory of electric, magnetic, and toroidal polarizations in crystalline solids with applications to hexagonal lonsdaleite and cubic diamond. *Phys. Rev. B* **107**, 155201 (2023).
27. Suzuki, M. T., Koretsune, T., Ochi, M. & Arita, R. Cluster multipole theory for anomalous Hall effect in antiferromagnets. *Phys. Rev. B: Condens. Matter Mater. Phys.* **95**, 094406 (2017).
28. Ghose, S. & Wan, C. Strong site preference of Co^{2+} in olivine, $\text{Co}_{1.10}\text{Mg}_{0.90}\text{SiO}_4$. *Contrib. Mineral. Petrol.* **47**, 131–140 (1974).
29. Morimoto, N., Tokonami, M., Watanabe, M. & Koto, K. Crystal structures of three polymorphs of Co_2SiO_4 . *Am. Mineral.* **59**, 475–485 (1974).
30. Sazonov, A. *et al.* Anomalous thermal expansion of cobalt olivine, Co_2SiO_4 , at low temperatures. *J. Appl. Crystallogr.* **43**, 720–728 (2010).
31. Lottermoser, W. & Fuess, H. Magnetic structure of the orthosilicates Mn_2SiO_4 and Co_2SiO_4 . *phys. stat. sol. (a)* **109**, 589–595 (1988).
32. Ballet, O. *et al.* Magnetisation measurements of the synthetic olivine single crystals A_2SiO_4 with $\text{A}=\text{Mn}$, Fe or Co . *J. Phys. Condens. Matter* **1**, 4955 (1989).
33. Sazonov, A. *et al.* Magnetic behaviour of synthetic Co_2SiO_4 . *Acta Crystallogr. B* **65**, 664–675 (2009).
34. Birss, R. R. *Symmetry & Magnetism*. (North-holland publishing company, Amsterdam, 1966).
35. Kimura, K. & Kimura, T. Nonvolatile Switching of Large Nonreciprocal Optical Absorption at Shortwave Infrared Wavelengths. *Phys. Rev. Lett.* **132**, 036901 (2024).
36. Smolyanyuk, A., Šmejkal, L. & Mazin, I. I. A tool to check whether a symmetry-compensated collinear magnetic material is antiferro- or altermagnetic. *arXiv:2401.08784* (2024).
37. Cheong, S.-W. & Huang, F.-T. Altermagnetism with non-collinear spins. *npj Quantum Materials* **9**, 1–6 (2024).
38. Jung, J. H. *et al.* Optical magnetoelectric effect in the polar GaFeO_3 ferrimagnet. *Phys. Rev. Lett.* **93**, 037403 (2004).
39. Kubota, M. *et al.* X-ray directional dichroism of a polar ferrimagnet. *Phys. Rev. Lett.* **92**, 137401 (2004).
40. Reschke, S. *et al.* Confirming the trilinear form of the optical magnetoelectric effect in the polar honeycomb antiferromagnet $\text{Co}_2\text{Mo}_3\text{O}_8$. *npj Quantum Mater.* **7**, 1 (2022).
41. Sato, T., Abe, N., Tokunaga, Y. & Arima, T. H. Antiferromagnetic domain wall dynamics in magnetoelectric MnTiO_3 studied by optical imaging. *Phys. Rev. B* **105**, 094417 (2022).
42. Kimura, K., Otake, Y. & Kimura, T. Visualizing rotation and reversal of the Néel vector through

- antiferromagnetic trichroism. *Nat. Commun.* **13**, 697 (2022).
43. Hayashida, T., Arakawa, K., Oshima, T., Kimura, K. & Kimura, T. Observation of antiferromagnetic domains in Cr₂O₃ using nonreciprocal optical effects. *Phys. Rev. Res.* **4**, 043063 (2022).
 44. Uemura, Y. *et al.* Field-Modulation Imaging of Ferroelectric Domains in Molecular Single-Crystal Films. *Phys. Rev. Appl.* **11**, 014046 (2019).
 45. Taran, M. N. & Rossman, G. R. Optical spectra of Co²⁺ in three synthetic silicate minerals. *Am. Mineral.* **86**, 889–895 (2001).
 46. Honda, T. *et al.* Coupled multiferroic domain switching in the canted conical spin spiral system Mn₂GeO₄. *Nat. Commun.* **8**, 15457 (2017).
 47. Leo, N. *et al.* Magnetoelectric inversion of domain patterns. *Nature* **560**, 466–470 (2018).
 48. Hassanpour, E. *et al.* Magnetoelectric transfer of a domain pattern. *Science* **377**, 1109–1112 (2022).
 49. Bhowal, S. & Spaldin, N. A. Ferroically Ordered Magnetic Octupoles in d-Wave Altermagnets. *Phys. Rev. X* **14**, 011019 (2024).
 50. Nakajima, T., Tokunaga, Y., Taguchi, Y., Tokura, Y. & Arima, T.-H. Piezomagnetoelectric Effect of Spin Origin in Dysprosium Orthoferrite. *Phys. Rev. Lett.* **115**, 197205 (2015).
 51. Dzialoshinskii, I. E. The problem of piezomagnetism. *Sov. Phys. JETP* **6**, 621–622 (1958).
 52. Borovik-Romanov, A. S. Piezomagnetism in antiferromagnetic cobalt and manganese fluorides. *J. Exptl. Theoret. Phys. (U.S.S.R.)* **36**, 1088–1098 (1959).
 53. Borovik-romanov, A. S. Piezomagnetism, linear magnetostriction and magneto optic effect. *Ferroelectrics* **162**, 153–159 (1994).
 54. Higuchi, T. & Kuwata-Gonokami, M. Control of antiferromagnetic domain distribution via polarization-dependent optical annealing. *Nat. Commun.* **7**, 10720 (2016).
 55. Kusunose, H. & Hayami, S. Generalization of microscopic multipoles and cross-correlated phenomena by their orderings. *J. Phys. Condens. Matter* **34**, 464002 (2022).
 56. Tang, Q. & Dieckmann, R. Floating-zone growth and characterization of single crystals of cobalt orthosilicate, Co₂SiO₄. *J. Cryst. Growth* **317**, 119–127 (2011).
 57. Momma, K. & Izumi, F. Vesta3 for threedimensional visualization of crystal, volumetric and morphology data. *J. Appl. Crystallogr.* **44**, 1272–1276 (2011).

Acknowledgments

We thank K. Kimura and T. Aoyama for fruitful discussions. The images of crystal structures were drawn using the software VESTA⁵⁷. This work was supported by JSPS 271 KAKENHI Grants No. JP19H05823 and No. JP21H04436.

Author Contributions

T.H. and K.M. equally contributed to this work. T.H. and T.K. designed the research. K.M. performed experiments and analyzed data under the guidance of T.H.. T.H. and T.K. prepared the manuscript, and all authors discussed and contributed to the final manuscript.

Competing interests

The authors declare no competing interests.

Data availability

The data presented in this paper are available from the corresponding authors on reasonable request.

ORCIDi

Takeshi Hayashida 0000-0002-9395-4254

Tsuyoshi Kimura 0000-0002-8030-5538

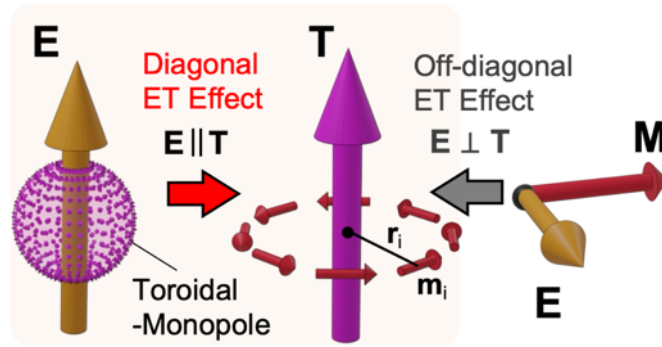


Figure 1: Magnetic toroidal moment and electrotoroidic (ET) effect. Magnetic toroidal moment \mathbf{T} is composed of vortex arrangements of magnetic dipoles \mathbf{m}_i (middle panel). \mathbf{T} can be induced by an electric field \mathbf{E} as a result of the ET effect. The off-diagonal ET effect refers to \mathbf{T} induced perpendicular to \mathbf{E} ($\mathbf{E} \perp \mathbf{T}$), which is achieved by a cross-product of magnetization \mathbf{M} and an applied \mathbf{E} , $\mathbf{T} \propto \mathbf{M} \times \mathbf{E}$ (right panel). The diagonal ET effect, \mathbf{T} induced parallel to \mathbf{E} ($\mathbf{E} \parallel \mathbf{T}$), is mediated by a T -odd scalar quantity, such as magnetic toroidal monopole (left panel).

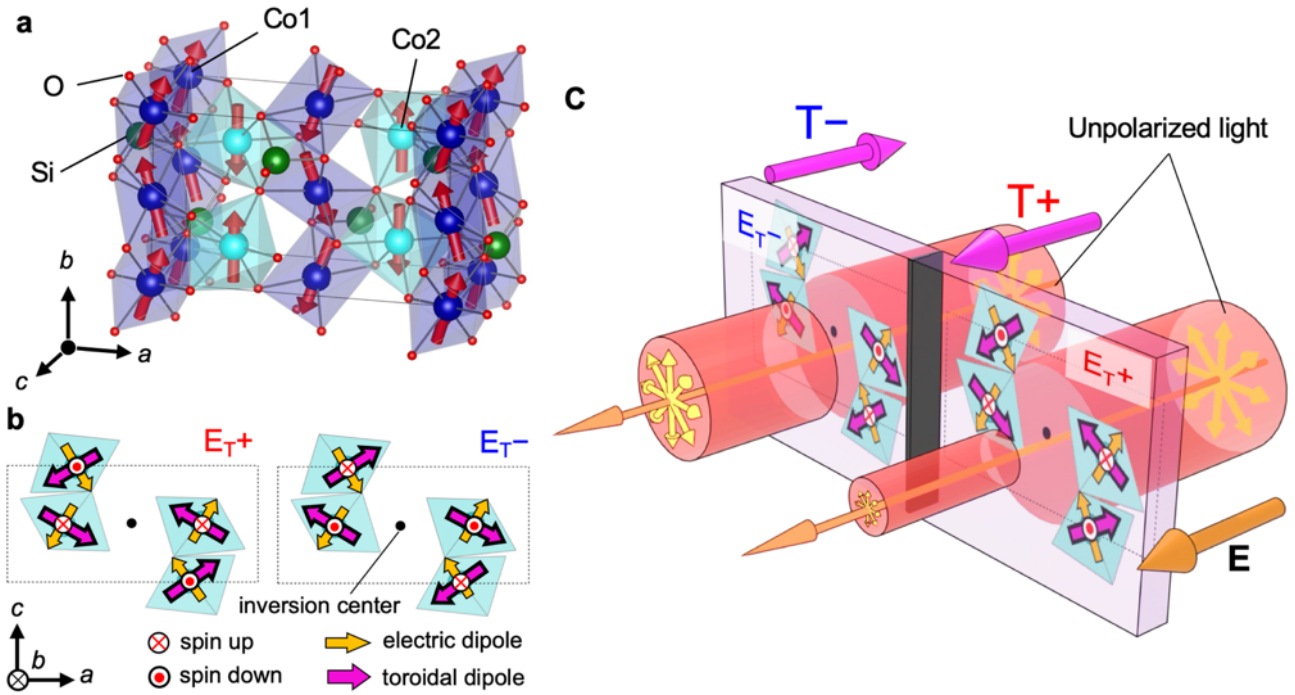


Figure 2: Magnetic structure and electric-field-induced nonreciprocal dichroism (E -induced NDD) in Co_2SiO_4 .

a, Crystal and magnetic structures of Co_2SiO_4 . The red arrows denote Co^{2+} spins. **b**, Two magnetic domain states (E_{T+} and E_{T-}) related to one another via time-reversal operation. For clarity, only CoO_6 octahedral units at the $\text{Co}2$ sites are shown. The circles with red dots or crosses in the center, yellow arrows, and magenta arrows denote local spins, electric dipoles, and magnetic toroidal dipoles, respectively. The E_{T+} and E_{T-} domain states are characterized by magnetic toroidal monopoles with a positive ($\sum_i \mathbf{r}_i \cdot \mathbf{t}_i > 0$) and negative ($\sum_i \mathbf{r}_i \cdot \mathbf{t}_i < 0$) divergence of \mathbf{t} , respectively. The dashed box denotes a unit cell. **c**, E -induced NDD in Co_2SiO_4 . Under an electric field \mathbf{E} , the E_{T+} and E_{T-} domain states exhibit magnetic toroidal moments with the opposite polarities ($T+$ and $T-$), resulting in an absorption difference of unpolarized light. Although here we depict the model in the setting of $\mathbf{E} \parallel \mathbf{k} \parallel b$, E -induced NDD is permitted in any direction if $\mathbf{E} \parallel \mathbf{k}$ is satisfied.

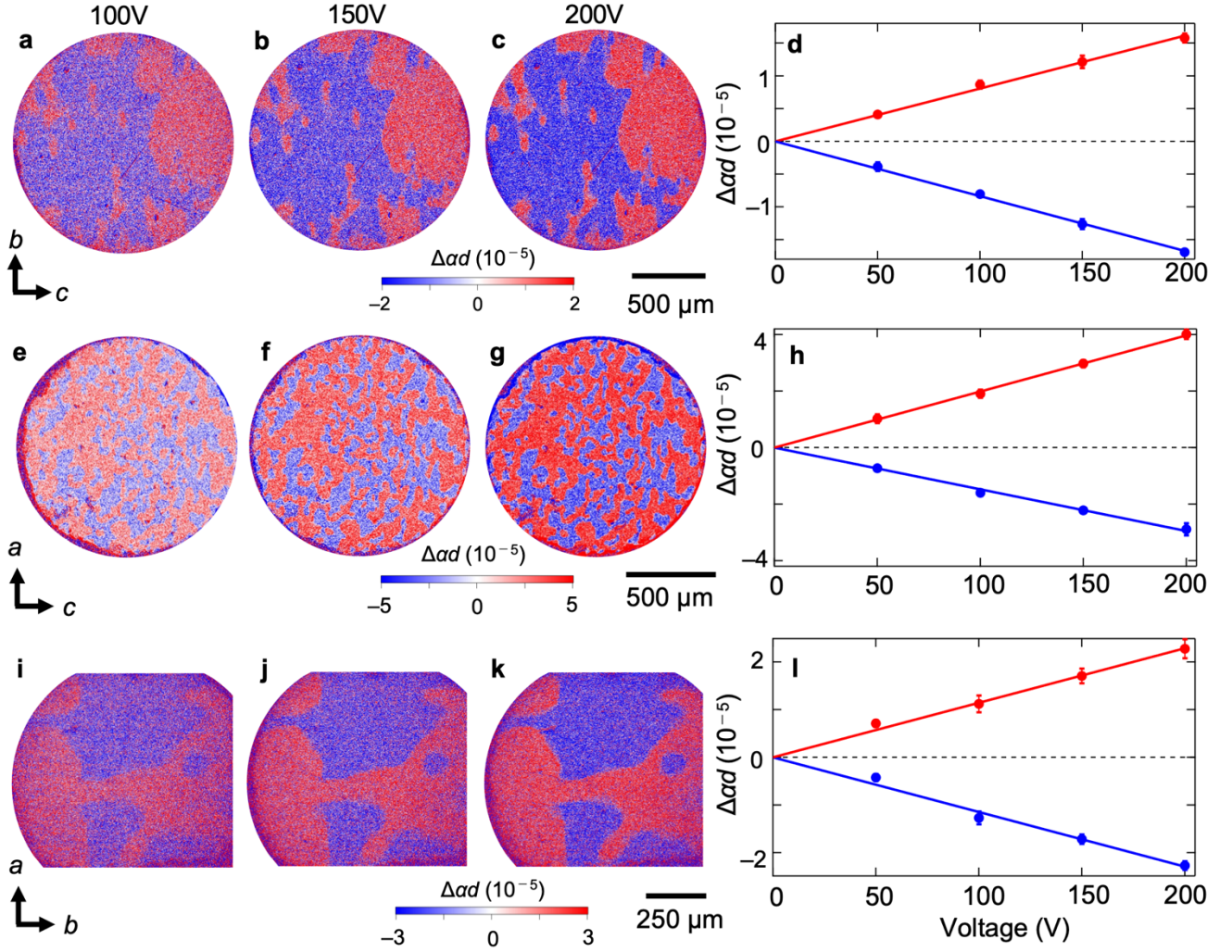


Figure 3: E_T domains observed by E -induced NDD. Panels a-c, e-g, and i-k show maps of changes in the absorption of unpolarized light ($\Delta\alpha d$) induced by applying voltage in the (100), (010), and (001) planes, respectively. The first (a,e,i), second (b,f,j), and third (c,g,k) columns show the images obtained under applied voltages of 100, 150, and 200 V, respectively. The applied voltage and light propagation direction \mathbf{k} were parallel to the normal axis of each plane. The wavelengths of the incident light were 550 nm (a-c and i-k) and 590 nm (e-g). The images were obtained at 4 K. Panels d, h, and I show the voltage dependence of the $\Delta\alpha d$ averaged in 10 different points for each domain state in the (100), (010), and (001) planes, respectively. The sampling positions are shown in Fig. S1. The red and blue dots correspond to the data for the positive and negative $\Delta\alpha d$ single domain areas, respectively. The error bars show the standard deviations for the 10 points. The lines denote the least-squares fitting lines.

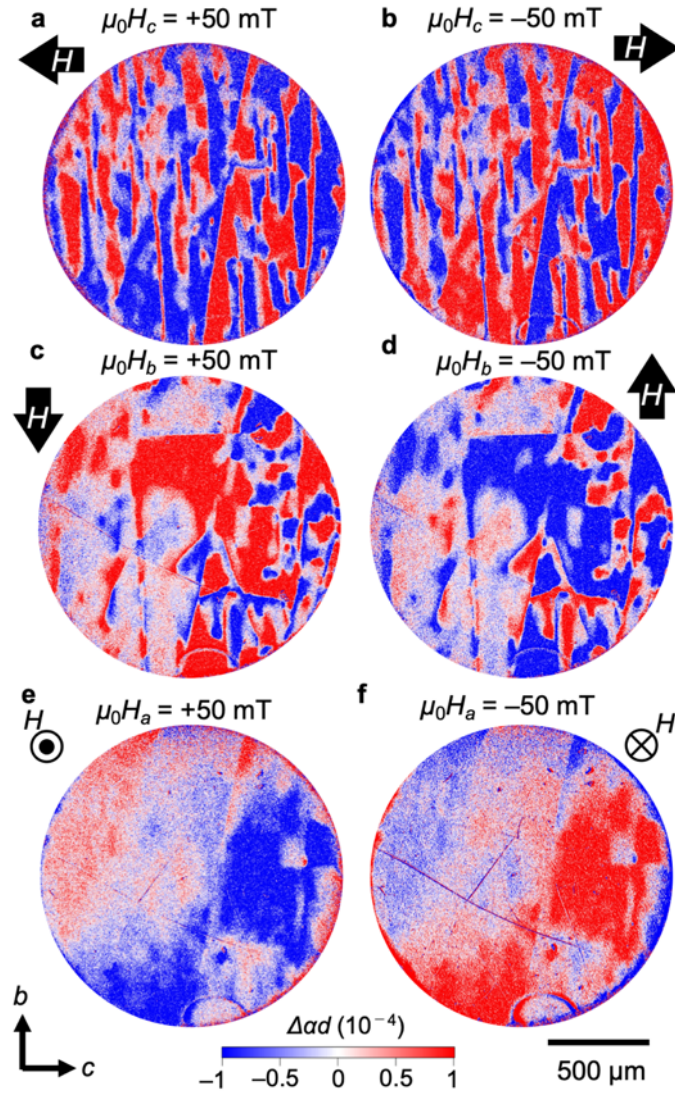


Figure 4: E_T domain inversion by applying a magnetic field. a-f, E_T domains in the (100) plane obtained at 4 K in the absence of a magnetic field after cooling the sample across T_N in a magnetic field of ± 50 mT along the c axis (a,b), b axis (c,d) and a axis (e,f); c -polarized light with a wavelength of 590 nm was used for imaging, and the applied voltage was 200 V. The domains obtained by applying positive and negative magnetic fields show the same pattern, but the contrast is inverted (a vs. b, c vs. d, and e vs. f).

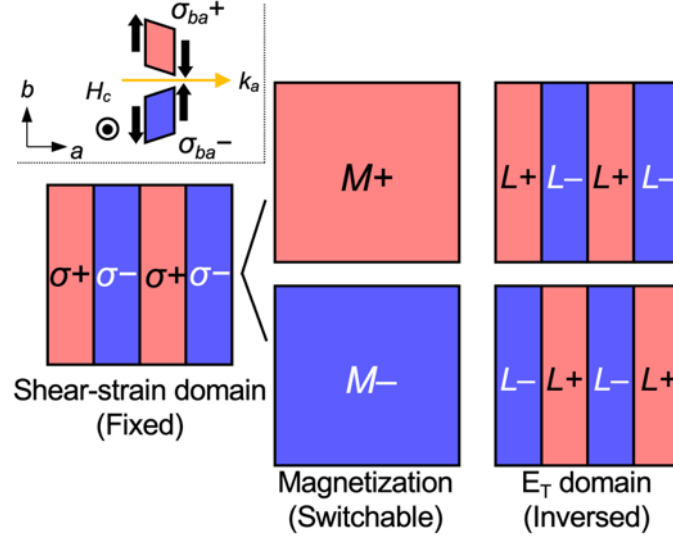
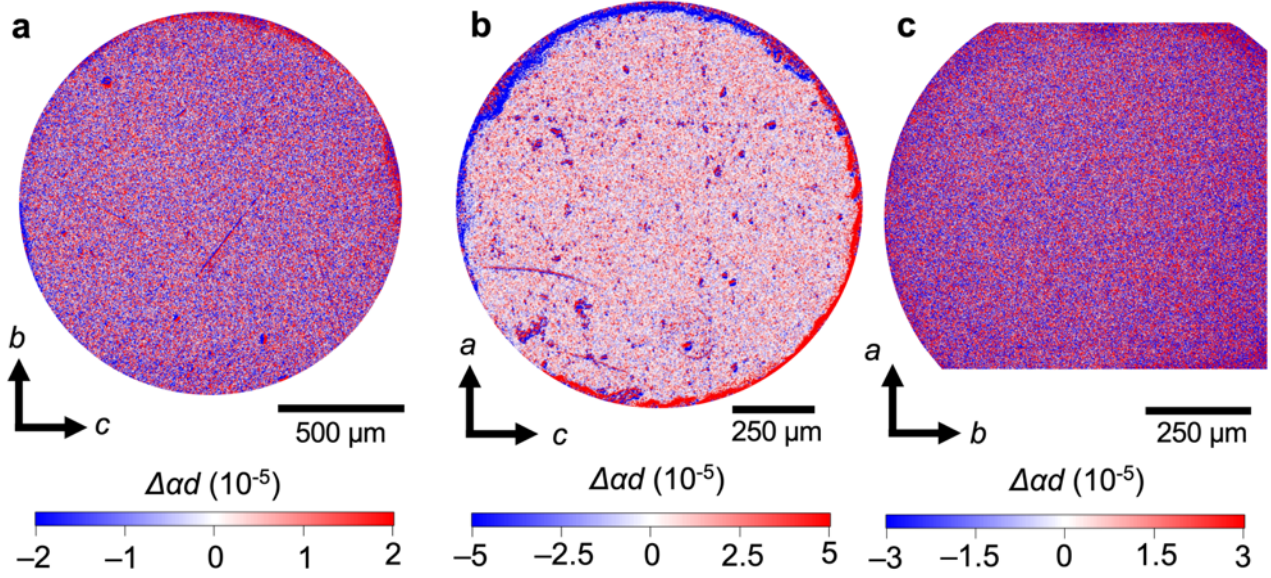
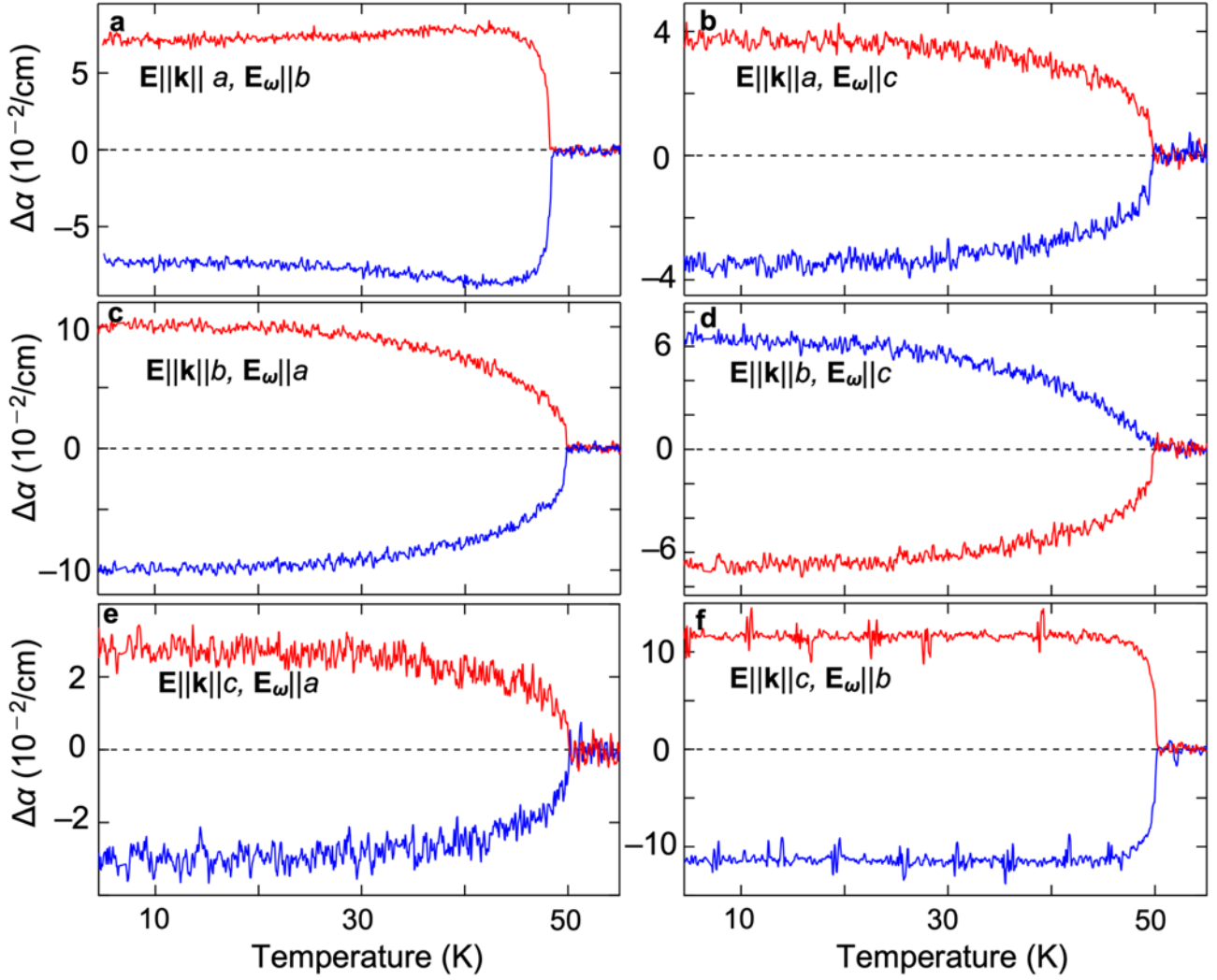


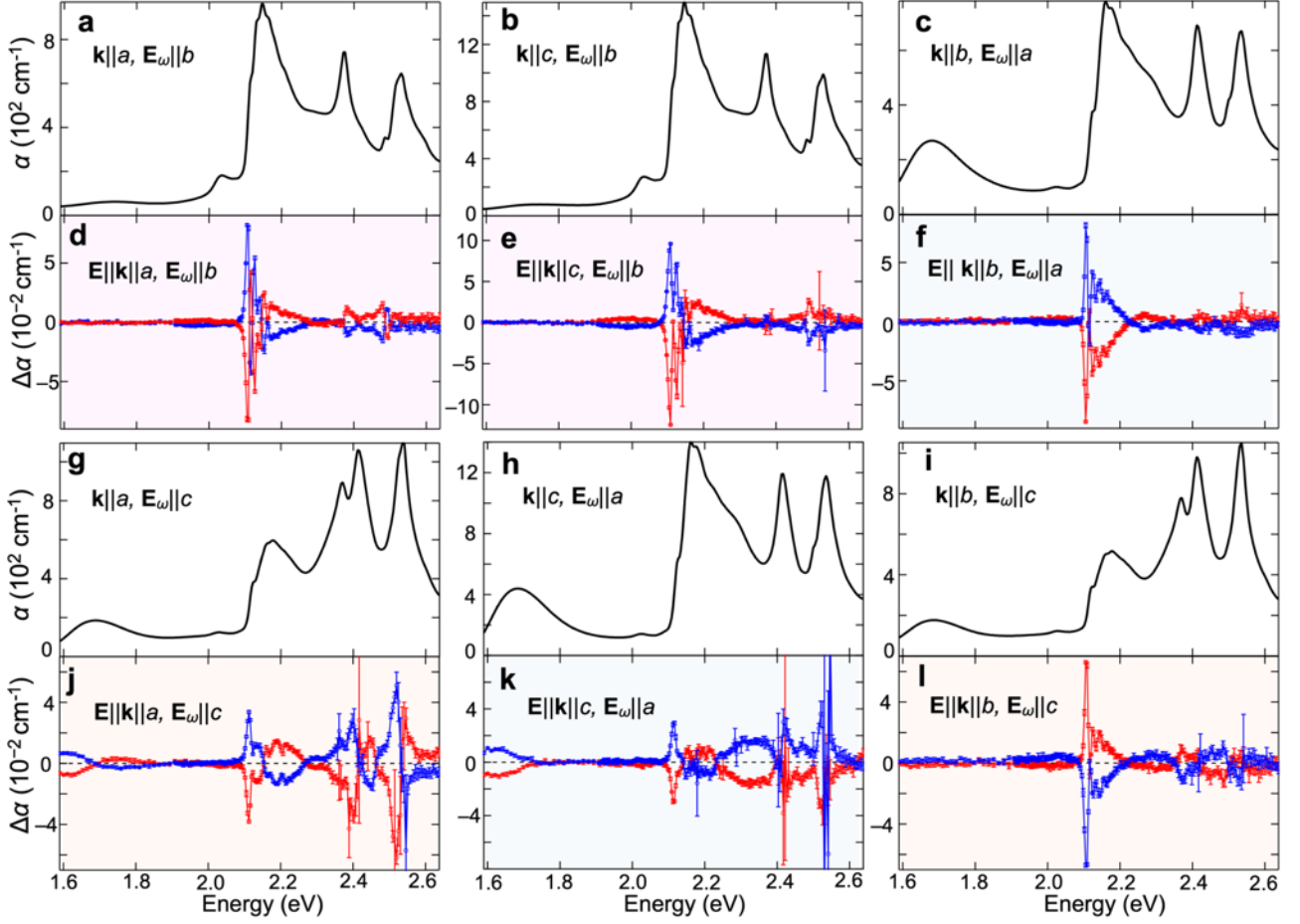
Figure 5: E_T domain inversion model with a trilinear coupling. Red and blue represent the positive and negative domain states for each order parameter (shear strain: σ , magnetization: M , E_T domain: L), respectively. The shear-strain domain remains rigid and invariant under a magnetic field (left panel). Thus, when a magnetic field is applied and magnetization is uniform ($M+$ or $M-$), the E_T domain pattern mirrors the shear-strain distribution. The sign of E_T domain is inverted for $M+$ and $M-$, to satisfy the trilinear coupling of $F = -\sigma ML$. The inset figure shows the situation corresponding to Fig. 4a, where the (100) plane domain is obtained with a magnetic field applied along the c axis. In this case, the distribution of σ_{ba} determines the E_T domain structure.



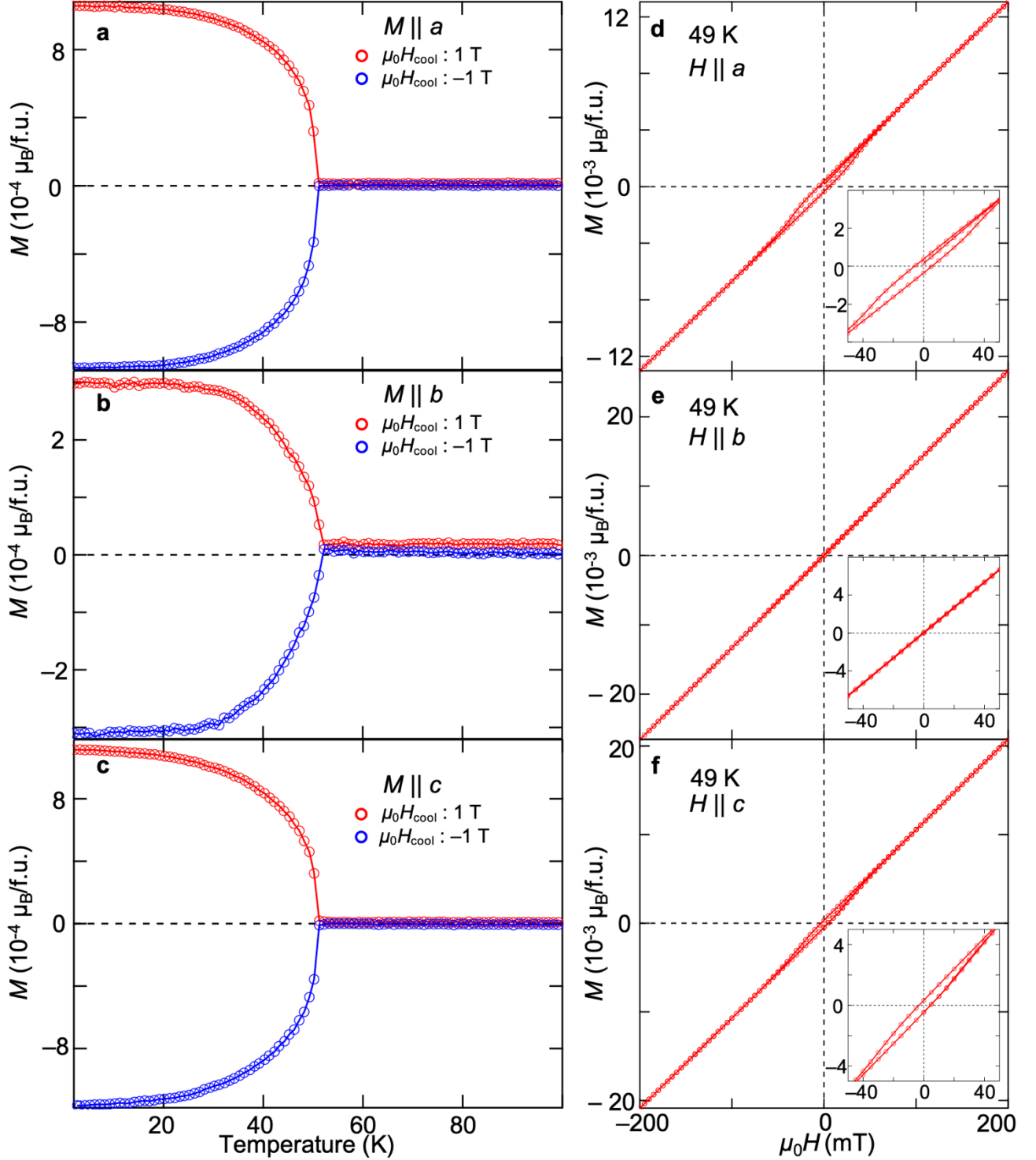
Extended Data Figure 1: Spatial distribution of E -induced NDD above T_N . Panels **a**, **b**, and **c** show the maps of changes in $\Delta\alpha d$ induced by an applied voltage of $V = 200$ V in the (100), (010), and (001) planes, respectively, at temperatures above $T_N = 50$ K (**a**:52 K, **b**:61 K, **c**:53 K). Applied electric field \mathbf{E} and light propagation direction \mathbf{k} are parallel to the normal axis of each plane. The wavelengths of the incident light are 550 nm (**a,c**) and 590 nm (**b**). The images in panels **a**, **b**, and **c** were taken at the same position on the same sample as those in Figs. 3**a-c**, **e-g**, and **i-k**.



Extended Data Figure 2: Temperature dependence of E -induced NDD. The temperature dependence of $\Delta\alpha$ at 150 V was obtained by focusing a laser beam on a single domain region and using a lock-in technique, with the sample temperature increasing at a rate of 1 K/min. Following the results of the spectral measurements (Extended Data Fig. 3), the wavelengths that maximized $\Delta\alpha$ were selected (588 nm for **a,f**, 587 nm for **b,e**, 589 nm for **c,d**). Panels **a(b)** show the temperature dependence of α and $\Delta\alpha$ for $b(c)$ -polarized light [$\mathbf{E}_\omega||b(c)$] propagating along the a axis ($\mathbf{k}||a$). In the same manner, panels **c(d)** show the temperature dependence for $\mathbf{k}||b$ and $\mathbf{E}_\omega||a(c)$, while panels **e(f)** show those for $\mathbf{k}||c$ and $\mathbf{E}_\omega||a(b)$. The red and blue correspond to the data obtained with either E_{T^+} or E_{T^-} domains. The results in two different \mathbf{E}_ω for the same \mathbf{k} obtained at the same domain state are represented by the same color. Except for panel **a**, the signals of E -induced NDD disappear at 50 K, corresponding to the antiferromagnetic transition. In panel **a**, the signal disappearance temperature is about 3 K lower, which was attributed to heating caused by irradiation with the focused laser.



Extended Data Figure 3: Spectra of E -induced NDD. **a-l**, Energy dependence of absorption coefficient α (**a-c** and **g-i**) and E -induced NDD $\Delta\alpha$ under 150 V (**d-f** and **j-l**) at 4 K. Here, for comparison with α , E -induced NDD is shown as $\Delta\alpha$, not $\Delta\alpha d$. Panels **a** and **d** (**g** and **j**) show the spectra of α and $\Delta\alpha$ for b (c)-polarized light [$\mathbf{E}_\omega \parallel b(c)$] propagating along the a axis ($\mathbf{k} \parallel a$), respectively. In the same manner, panels **b** and **e** (**g** and **j**) show the spectra for $\mathbf{k} \parallel c$ and $\mathbf{E}_\omega \parallel b(a)$, while panels **c** and **f** (**i** and **l**) show those for $\mathbf{k} \parallel b$ and $\mathbf{E}_\omega \parallel a(c)$. In the $\Delta\alpha$ spectra, the electric field \mathbf{E} is applied parallel to \mathbf{k} . The red and blue dots in the E -induced NDD spectra correspond to the data obtained for either E_{T+} or E_{T-} domains. The results in two different \mathbf{E}_ω for the same \mathbf{k} obtained at the same domain state are represented by the same color. The $\Delta\alpha$ spectra for the same direction of \mathbf{E}_ω are highlighted in the same color. Error bars show standard deviations.



Extended Data Figure 4: Magnetic properties of Co_2SiO_4 . a-c, Temperature dependence of spontaneous magnetization (M) along the a (a), b (b), and c (c) axes. The red and blue dots show the results measured after cooling the sample across T_N in a magnetic field (H) of 1 and -1 T , respectively. A small magnetic field up to $\pm 0.001 \text{ T}$ was applied during the measurements to suppress residual magnetic field. The offsets observed above T_N were attributed to residual magnetic field. d-f, Magnetization curves at 49 K (just below T_N) for H along the a (d), b (e), and c (f) axes. The insets show enlarged views of the range from -50 to 50 mT . Small spontaneous magnetization and hysteresis behaviors are observed for H along the a and c axes, but not for H along the b axis.

Supplementary Information for

**Electric-field-induced toroidal moment in a time-reversal-odd
antiferromagnet**

T. Hayashida¹, K. Matsumoto¹, and T. Kimura¹

¹*Department of Applied Physics, University of Tokyo, Tokyo 113-8656, Japan.*

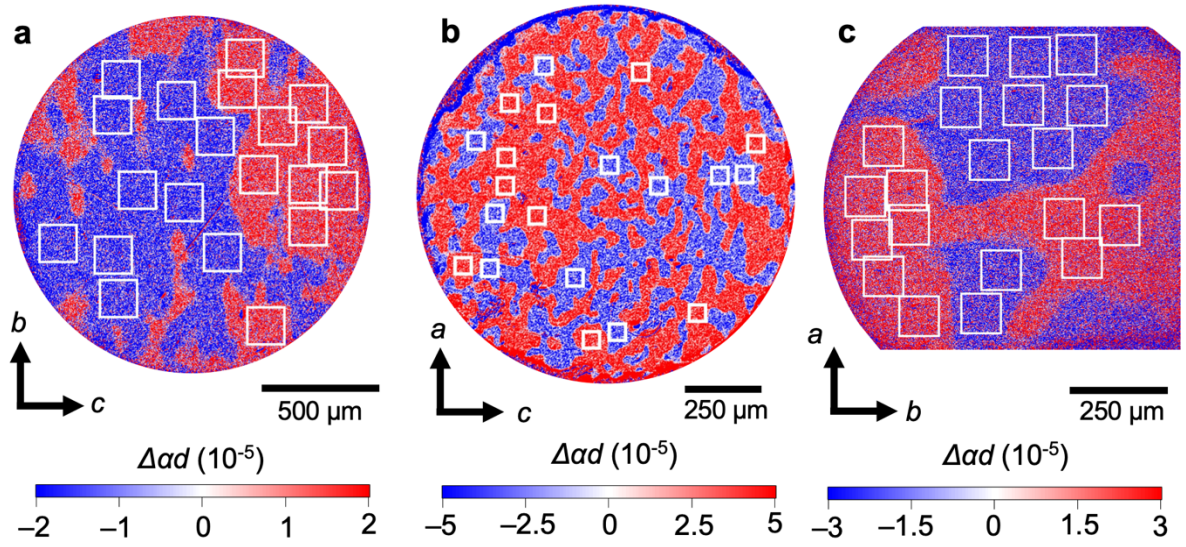


Figure S1: Sampling positions for calculating the voltage dependence of E -induced NDD. The white boxes in panels **a**, **b**, and **c** show the areas where the average of $\Delta\alpha d$ was obtained to calculate the voltage dependence of $\Delta\alpha d$ shown in Figs. 3d, h, and l in the main text, respectively.

Supplementary Note 1 | Details of E -induced NDD spectrum

Here we discuss the details of E -induced NDD spectrum. The obtained E -induced NDD spectra are shown again in Figs. S2d-f and S2j-l along with the absorption spectra (Figs. S2a-c and S2g-i). Here, the measurements in the two polarization settings of each \mathbf{k} direction were performed for the same domain state, and the red and blue dots denote the data obtained in either E_{T^+} or E_{T^-} domains. The E -induced NDD spectra taken at the opposite domains show a complete sign reversal. In Co_2SiO_4 , the absorption in the visible light region is mainly due to the Co^{2+} d - d transition¹. Among the two Co sites, the Co1 site in a centrosymmetric field does not significantly contribute to the absorption¹. Thus, we focus on the Co2 site in the following discussion. The absorption peaks observed around 2.0–2.6 eV are ascribed to the d - d transition from the ground state T_{1g} to the excited T_{1g} state. Here, T_{1g} refers to the state split by the cubic crystal field. Because of the effect of the distorted crystal field, it is further split into roughly three states. Around the same energy, the E -induced NDD shows complicated peak structures. In the following discussion, we do not delve into the details of all the peaks but consider a model to explain the origin of E -induced NDD in each setting from the overall features of the spectra. An important feature is that the spectra at $\mathbf{E}||\mathbf{k}||a$ and $\mathbf{E}_\omega||b$ (Fig. S2d) and those at $\mathbf{E}||\mathbf{k}||c$ and $\mathbf{E}_\omega||b$ (Fig. S2e) are quite similar, whereas those at $\mathbf{E}||\mathbf{k}||a$ and $\mathbf{E}_\omega||c$ (Fig. S2j) significantly differ from those at $\mathbf{E}||\mathbf{k}||b$ and $\mathbf{E}_\omega||c$ (Fig. S2i), and those at $\mathbf{E}||\mathbf{k}||c$ and $\mathbf{E}_\omega||a$ (Fig. S2k) from those at $\mathbf{E}||\mathbf{k}||b$ and $\mathbf{E}_\omega||a$ (Fig. S2f). The E -induced NDD spectra at $\mathbf{E}||\mathbf{k}||a,c$ have finer peak structures, where positive and negative signal swings are sharper than those at $\mathbf{E}||\mathbf{k}||b$. Because no significant differences are observed in the absorption spectra (Fig. S2g with S2i), the magnetic structure rather than structural anisotropy should determine the difference in the E -induced NDD spectra. This can be considered in a model based on the local toroidal moments as follows.

Let us first discuss the model for the E -induced NDD spectra at $\mathbf{E}||\mathbf{k}||b$. As illustrated in Fig. S2n, Co^{2+} spins at the Co2 site are parallel to the b axis so that a toroidal moment parallel to the b axis is not induced even if \mathbf{E} is applied. At finite \mathbf{E} , however, the mirror plane perpendicular to the b axis at each site is broken, resulting in a chiral state. When the system is chiral, a toroidal moment parallel to a magnetic moment is induced because of magneto-chiral coupling^{2,3}. Now, the two sites (X1 and X2) with up spins have the same chirality (let us assume a right-handed structure) when \mathbf{E} is applied, and the other two sites (Y1 and Y2) with down spins have left-handed chirality. The X sites have up spin and right-handed chirality, and the Y sites have down spin and left-handed chirality, i.e., the X and Y sites exhibit opposite spins and chirality. Because a local toroidal moment \mathbf{t} is the product of spin and chirality, the sites show the same polarity of induced \mathbf{t} . Accordingly, the appearance of E -induced NDD at $\mathbf{E}||\mathbf{k}||b$ can be interpreted as the sum of \mathbf{t} becoming finite under \mathbf{E} . With such a finite toroidal moment, the photon energy ($\hbar\omega$) dependence of NDD around a single excitation energy $\hbar\omega_{n0}$ is described as^{4,5}

$$\Delta\alpha(\omega) \propto \frac{\text{Re}[\langle 0|m_\beta|n\rangle\langle n|p_\alpha|0\rangle]}{(\omega - \omega_{n0})^2 + \delta_n^2} \quad (\text{S1})$$

where $\langle 0|m_\beta|n\rangle$ and $\langle n|p_\alpha|0\rangle$ are matrix elements of magnetic (m_β) and electric (p_α) dipole operators, respectively, taken between the ground $|0\rangle$ and the excited states $|n\rangle$ separated by $\hbar\omega_{n0}$ energy; α and β specify the directions of the electric and magnetic fields of light, respectively; δ_n is the

inverse lifetime of the excited state $|n\rangle$. According to this equation, $\Delta\alpha(\omega)$ has an absorptive structure with a single peak at ω_{n0} , which is roughly consistent with the spectra shown in Fig. S2f,l.

Let us now consider E -induced NDD at $\mathbf{E}||\mathbf{k}||a,c$. As mentioned above, \mathbf{t} at each Co2 site is finite along the a and c axes in $\mathbf{E}||a$ and $\mathbf{E}||c$, respectively. Although the sum of \mathbf{t} in a unit cell is canceled out, the application of \mathbf{E} along a or c induces a net toroidal moment along the same direction of \mathbf{E} . However, this net toroidal moment is not a major contributor to the NDD at the resonance energy. Instead, the difference between mutually antiparallel local toroidal moments is a determining factor. Let us take the X site as an example. Owing to the presence of local toroidal moments, NDD occurs locally, but the effects cancel each other out at X1 and X2. However, when \mathbf{E} is applied, the excitation energy that induces $\Delta\alpha$ changes linearly with respect to \mathbf{E} ($\Delta_E \propto |\mathbf{E}|$), where the sign of Δ_E is opposite at the X1 and X2 sites (pseudo-Stark effect)^{6,7}. As a result, the peak energies of NDD at the X1 and X2 sites become slightly different, so that they no longer cancel out, resulting in a finite NDD. The same process occurs at the Y1 and Y2 sites. This behavior, taking the pseudo-Stark effect into account, may be described as follows:

$$\begin{aligned} \Delta\alpha(\omega) &= \Delta\alpha^{X1}(\omega) - \Delta\alpha^{X2}(\omega) \\ &\propto \text{Re}[\langle 0|m_\beta|n\rangle\langle n|p_\alpha|0\rangle] \left\{ \frac{1}{[\omega - (\omega_{n0} + \Delta_E)]^2 + \delta_n^2} - \frac{1}{[\omega - (\omega_{n0} - \Delta_E)]^2 + \delta_n^2} \right\} \\ &\approx \text{Re}[\langle 0|m_\beta|n\rangle\langle n|p_\alpha|0\rangle] \frac{\omega - \omega_{n0}}{[(\omega - \omega_{n0})^2 + \delta^2]^2} \Delta_E. \end{aligned} \quad (\text{S2})$$

In this case, $\Delta\alpha(\omega)$ is proportional to $1/(\omega - \omega_{n0})^3$ and shows a dispersive structure with two peaks of opposite signs around the resonance frequency ω_{n0} , which is roughly consistent with the spectra shown in Fig. S2d,e,j,k. Therefore, in the resonance energy region, the existence of these antiparallel toroidal moments has a stronger effect on E -induced NDD than the finite sum of toroidal moments under \mathbf{E} .

Considering the above, the difference in the shape of the E -induced NDD spectra at $\mathbf{E}||\mathbf{k}||a,c$ and $\mathbf{E}||\mathbf{k}||b$ can be roughly explained. However, this explanation does not take into account the contribution of the spins on the Co1 site and the effect of orbital hybridization due to spin-orbit coupling⁸, which can be another factor in the dispersive peak structure, as a more detailed spectral analysis would be required to account for them.

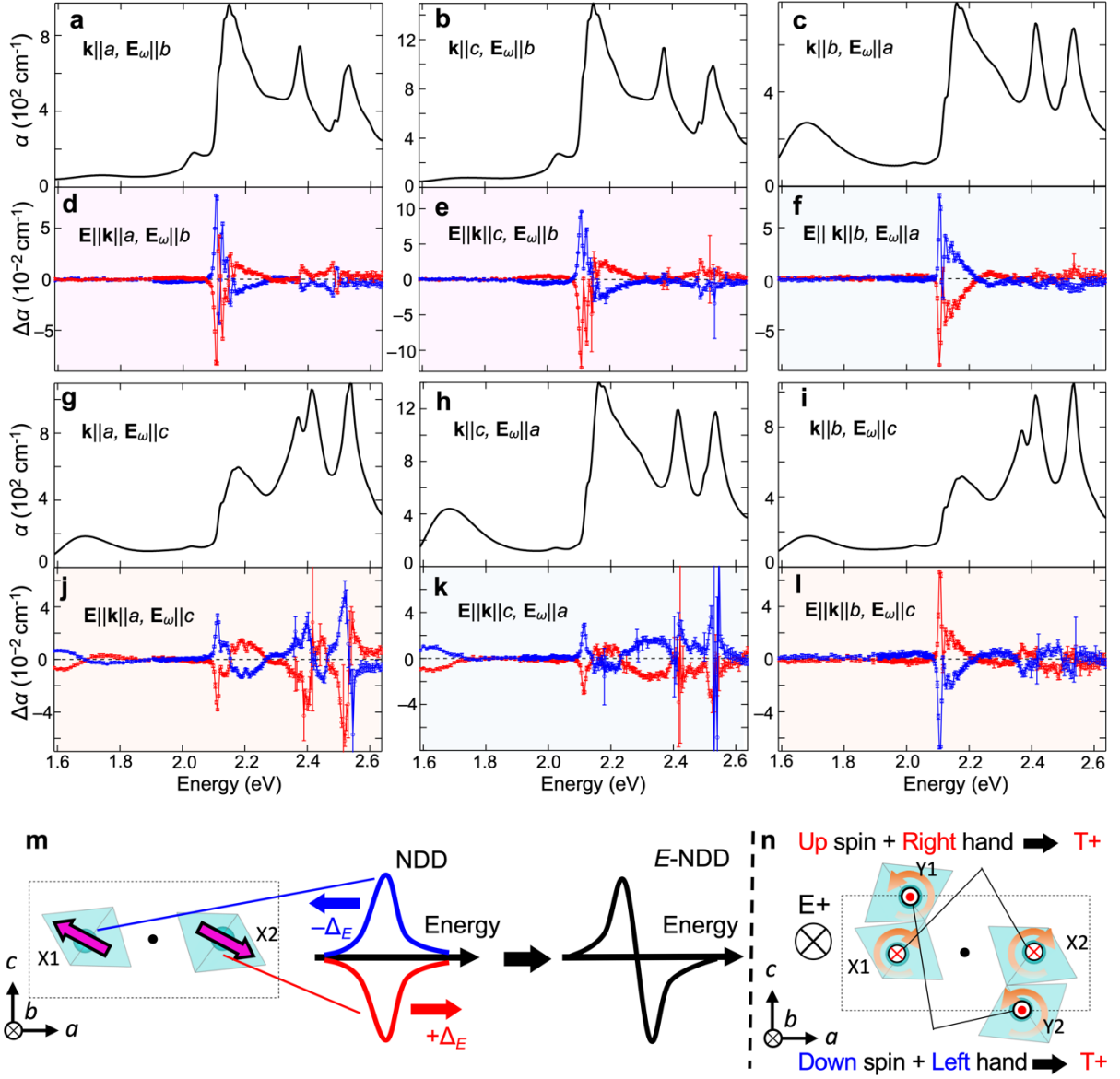


Figure S2: Spectra of E -induced NDD. a-l, Energy dependence of an absorption coefficient α (a-c and g-i) and E -induced NDD $\Delta\alpha$ under 150 V (d-f and j-l) at 4 K. Reproduced from Extended Data Fig. 3a-l. m, Model for the E -induced NDD in the case of $\mathbf{E}||\mathbf{k}||\mathbf{a}$ or \mathbf{c} . Although the local toroidal moments at X sites (magenta arrows) locally induce NDD, the contributions of X1 and X2 sites cancel each other out in the absence of an electric field. However, under an electric field, the resonance energy of the E -induced NDD is shifted in opposite sign ($\pm\Delta_E$), which induces finite NDD. n, Model for the E -induced toroidal moment in the case of $\mathbf{E}||\mathbf{k}||\mathbf{b}$. An electric field induces chirality at sites X and Y with opposite handedness. The toroidal moment is induced by the coupling of local spins and chirality. As the spins of sites X and Y are opposite, the signs of the toroidal moments at these sites are the same.

Supplementary Note 2 | E_T domain inversion by sweeping a magnetic field

In the (100) plane at 49 K (just below T_N), we performed the domain imaging with sweeping the magnetic field along the c axis as $0\text{ T} \rightarrow 200\text{ mT} \rightarrow -200\text{ mT} \rightarrow 200\text{ mT}$. Figure S3 shows the summary of the results. By applying just 50 mT, the domain patterns changed, as the number of domain walls perpendicular to the c axis ($dw \perp c$) increased (compare Fig. S3a with S3b). When the magnetic field was increased to 200 mT, this tendency became more pronounced (Fig. S3c). One finds that the domain contrast at 200 mT is somewhat whitish, which suggests that tiny regions with weak signals, for example, tiny multi- E_T domains smaller than the microscope resolution (several μm), spread throughout the sample. With decreasing H , the domain structure started changing again in between 50 mT and 0 T. After flipping the direction of the magnetic field, the same tendency of the increasing $dw \perp c$ with increasing H was observed. However, the domain contrast gets inverted with maintaining the pattern from that under $+H$ (compare Fig. S3e with Fig. S3c). The H dependence of $\Delta\alpha d$ averaged in one selected area surrounded by a black box in Fig. S3a shows a hysteresis loop (Fig. S3f). The coercive magnetic field is $10 \sim 20\text{ mT}$, which does not contradict the magnetization measurement where the coercive magnetic field is $5 \sim 10\text{ mT}$ at 49 K (see Fig. S3g). The magnitude of $|M|$ increases in proportion to $|H|$, whereas the magnitude of $|\Delta\alpha d|$ begins to decrease above $|\mu_0 H| = 20\text{ mT}$. This is most likely because as H is increased, regions with smaller strains respond to H , forming multidomains that are smaller than the resolution limit of the microscope (for the relationship between strain and magnetic field, see Main text).

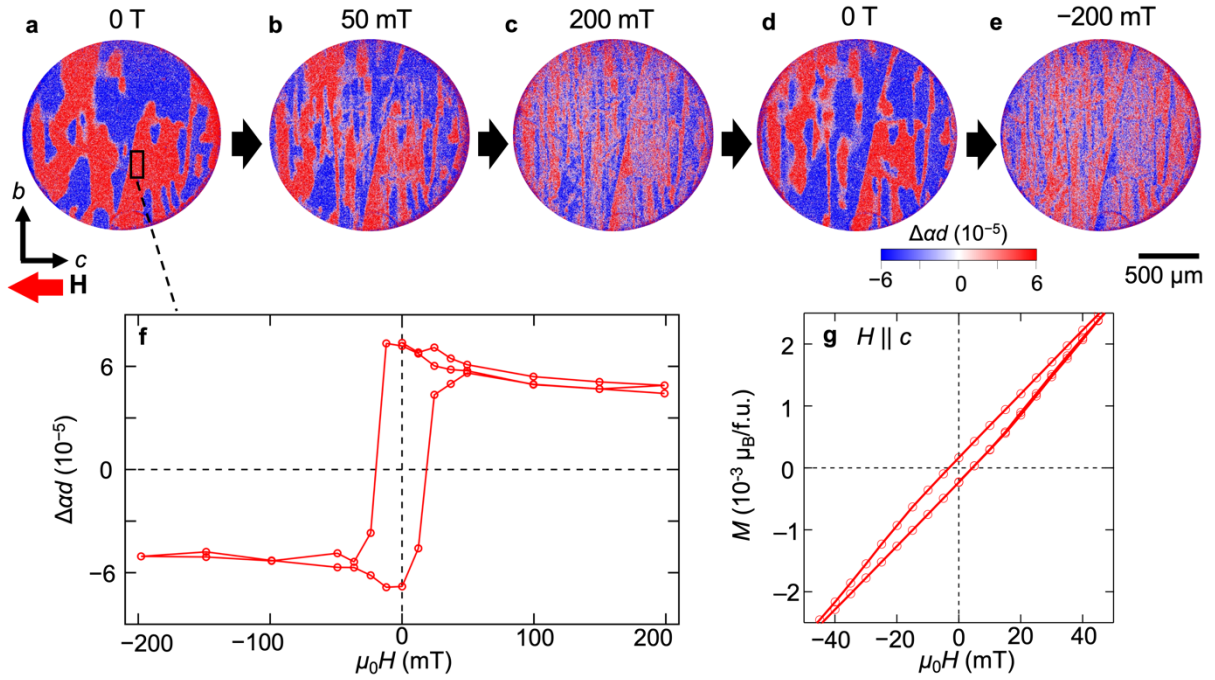


Figure S3: E_T domain inversion by sweeping a magnetic field. a-e, E_T domains in the (100) plane obtained while sweeping the magnetic field H applied along the c axis as 0 T \rightarrow 200 mT \rightarrow -200 mT \rightarrow 200 mT. The measurements were performed at 49 K ($< T_N$). The magnetic field was kept constant during each domain imaging. The b -polarized light with the wavelength of 590 nm was used for the imaging and the applied voltage was 200 V. When one compares the domains at 200 mT (c) and -200 mT (e), the pattern is the same, but the contrast is inverted. One also finds that the domain contrast at 200 mT (c) and -200 mT (e) is somewhat whitish, which suggests that tiny regions with weak signals, for example, tiny multi-E_T domains smaller than the microscope resolution (several μm), spread throughout the sample. f, H dependence of $\Delta\alpha d$ averaged in the areas surrounded by the black box in panel a. It shows a hysteresis behavior. g, Magnetization curves at 49 K for H along the c axis. Reproduced from the inset of Extended Data Fig. 4f.

Supplementary Reference

1. Taras, M. N. & Rossman, G. R. Optical spectra of Co^{2+} in three synthetic silicate minerals. *Am. Mineral.* **86**, 889–895 (2001).
2. Sato, T., Abe, N., Kimura, S., Tokunaga, Y. & Arima, T.-H. Magnetochiral Dichroism in a Collinear Antiferromagnet with No Magnetization. *Phys. Rev. Lett.* **124**, 217402 (2020).
3. Cheong, S.-W., Lim, S., Du, K. & Huang, F.-T. Permutable SOS (symmetry operational similarity). *npj Quantum Mater.* **6**, 58 (2021).
4. Kézsmárki, I. *et al.* One-way transparency of four-coloured spin-wave excitations in multiferroic materials. *Nat. Commun.* **5**, 3203 (2014).
5. Yokosuk, M. O. *et al.* Nonreciprocal directional dichroism of a chiral magnet in the visible range. *npj Quantum Mater.* **5**, 20 (2020).
6. Kaiser, W., Sugano, S. & Wood, D. L. Splitting of the emission lines of ruby by an external electric field. *Phys. Rev. Lett.* **6**, 605–607 (1961).
7. Krichevtsov, B. B., Pavlov, V. V. & Pisarev, R. V. Nonreciprocal optical effects in antiferromagnetic Cr_2O_3 subjected to electric and magnetic fields. *Zh. Eksp. Teor. Fiz* **94**, 284–295 (1988).
8. Arima, T. Magneto-electric optics in non-centrosymmetric ferromagnets. *J. Phys. Condens. Matter* **20**, 434211 (2008).